CFD analysis of melting process in a shell-and-tube latent heat storage for concentrated solar power plants

CFD ANALYSIS OF MELTING PROCESS IN A SHELL-AND-TUBE LATENT HEAT STORAGE FOR CONCENTRATED SOLAR POWER PLANTS

F. Fornarelli[1], S.M. Camporeale[1], B. Fortunato[1], M. Torresi[1], P. Oresta[1], L. Magliocchetti[1], A. Miliozzi[2], G. Santo[1]*

[1] Politecnico di Bari, Dipartimento di Ingegneria Meccanica, Matematica e Management, Sezione di Macchine ed Energetica, Via Orabona 4, 70125 Bari, Italy

[2]ENEA – Italian National Agency for New Technologies, Energy and Sustainable Economic Development,
Casaccia Research Centre, Via Anguillarese, 301 – 00123 S. Maria di Galeria, Rome, Italy

*Corresponding author. E-mail: francesco.fornarelli@poliba.it

HIGHLIGHTS

- Numerical simulation of the melting process in vertical latent heat storage device.
- Shell and tube heat storage device for CSP (Concentrated Solar Power) applications.
- Conjugate heat transfer model including HTF, steel tube, and PCM.
- Comparison of the results obtained from convective and pure conductive models.
- Influence of the mushy zone constant, A_{mush}, on enthalpy-porosity model.

ABSTRACT

A latent heat storage system for Concentrated Solar Plants (CSP) is numerically examined by means of CFD simulations. This study aims at identifying the convective flows produced within the melted phase by temperature gradients and gravity. Simulations were carried out on experimental devices for applications to high temperature concentrated solar power plants. A shell-and-tube geometry composed by a vertical cylindrical tank, filled by a Phase Change Material (PCM) and an inner steel tube, in which the heat transfer fluid (HTF) flows, from the top to the bottom, is considered. The conjugate heat transfer process is examined by

solving the unsteady Navier-Stokes equations for HTF and PCM and conduction for the tube. In order to take into account the buoyancy effects in the PCM tank the Boussinesq approximation is adopted. The results show that the enhanced heat flux, due to natural convective flow, reduce of about 30% the time needed to charge the heat storage. A detailed description of the convective motion in the melted phase and the heat flux distribution between the HTF and PCM are reported. The effect of the mushy zone constant is also investigated.

KEYWORDS:

CFD, thermal energy storage (TES), phase change material (PCM), molten salts, shell and tube, enthalpy-porosity model.

1. INTRODUCTION

Among electricity production systems based on renewable energy sources, in a medium-term perspective, Concentrated Solar Power (CSP) systems can give a significant contribution to the development of a sustainable electricity production [1]. CSP plants use solar energy as the main or the only heat source for energy production. Appropriate optical systems (concentrators) collect the direct solar radiation concentrating it on a receiver, where it is absorbed, and then converted into heat at high temperature, which is carried by means of a heat transfer fluid (HTF). CSP systems may be employed both in thermal cycles for electricity production and in various industrial applications as heat source [2].

The primary objective of the research on CSP systems is cost reduction, making both large and small size CSP plants more and more competitive with respect to conventional power plants based on fossil fuels. Currently the research aims not only at improving the efficiency

of both the main components and the entire system, but also to the simplification of the systems and the procedures for operation and maintenance. A key technological issue for CSP plants is the integration of an economic Thermal Energy Storage (TES) ([3], [4], [5] and [6]) with the overall objective to improve the operational flexibility and to reduce the Levelized Energy Cost (LEC) by increasing the share of solar energy being used [7].

Latent Heat Thermal Energy Storage (LHTES) Systems using Phase Change Materials (PCMs) have been gaining importance in several fields such as solar energy, cooling systems, energy efficiency buildings [8][9][10][11], cool storage systems for centralized air-conditioning systems and waste heat recovery systems [12]. Recently, several works have highlighted the development of mobilized thermal energy storage systems (M-TES), which represent a valid alternative to district heating pipelines in residential applications [14][15][16][17]. This is mainly due to their high energy storage density and their ability to provide heat at a constant temperature [18]. Since the latent heat of fusion of a PCM is high compared to the sensible heat, TES systems based on PCMs can be significantly smaller with respect to systems based on sensible heat. Due to the high working temperature of CSP applications (about 250°C), eutectic molten salts, that change phase at about 230°C, can be used and represent a good compromise in term of storable latent heat and material cost, as suggested by Sharma et al. [19], with respect to other TES that operates in the same range of temperatures, such as concrete and rock bed.

An LHTES system consists actually in the following three main components: (i) a PCM suitable for the desired temperature range; (ii) a container for the PCM; (iii) a heat exchange system in order to transfer the heat from the source to the PCM and then from the PCM to

the heat sink. The PCM containment should: (i) meet the requirements of strength, flexibility, corrosion resistance and thermal stability; (ii) act as a barrier to protect the PCM from harmful interaction with the environment; (iii) provide sufficient surface for heat transfer; (iv) provide structural stability and easy handling.

The main technological problem for the development of LHTES systems is the low thermal conductivities. The eutectic molten salts provide thermal conductivities ranging from 0.5 up to 1 W/(mK). Therefore, the design process of a heat exchanger is dominated by the identification of effective solutions in order to increase the heat flux inside the storage material. For instance, much effort has been devoted to improve the thermal exchange process of PCMs. Sciacovelli et al.[13] and Fan and Khodadadi [21] have considered the shell and tube configuration with fins immersed in the PCM. Sciacovelli et al. developed a numerical approach to optimize the fins shape within the PCM in order to maximize the heat exchange during the solidification process. The PCM has been modelled using a pure conductive heat exchange model, therefor the convective contribution to the heat exchange has been neglected. Sharma et al.[19] and Sharma and Sagara [20], in their review papers, classified a wide range of latent heat storage materials in order to provide an overview of the available PCMs and suggests different design solutions in order to enhance the heat exchange according to the specific application. Another approach to increase the heat exchange within the PCM is the use of metal foams, as proposed by Zhao and Wu [22], which, however, increase significantly weights and costs.

Recently, Seddegh et al. [23] investigated numerically the behavior of a shell and tube TES system, considering water as HTF and paraffin wax as PCM. They highlight the

importance of convective heat transfer especially during the melting process. In their numerical setup the heat transfer at the inner surface of the PCM has been modelled according to the HTF flow condition (fully turbulent). Guo et al. [16] investigated numerically various approach in order to reduce the charging time of an M-TES device. In their work, details of the convective motion within the melted PCM are reported highlighting how the convective PCM motion could affect the charging process. The M-TES device studied by Guo et al. involves a direct contact between the HTF and the PCM. The geometry consist in a cylinder with the axis perpendicular respect to the gravity acceleration. In this configuration the convective motion involves both the phases that due to the different buoyancy stratify in two different zones of the device. Even though the results are promising in terms of charging time, however the geometry proposed and the direct contact heat exchange imply a physical behavior completely different respect to the shell-and-tube device here studied.

The scope of the present work is to study the heat exchange characteristics in a basic shell and tube latent heat thermal storage system for CSP plants operating at medium temperature (200-250°C), through CFD modeling. Respect to previous investigation the shell and tube device has been modelled solving the Navier-Stokes equation for both the phases, HTF and PCM, with an enthalpy-porosity model for the melting process. The heat flux between the two phases has not be approximated by simplified models therefor a calculated heat flux distribution along the longitudinal coordinate. The effect of convection in PCM has been evaluated by means of a comparison with a pure conductive model. The PCM, selected for this study, is a binary eutectic salt ($NaNO_3$-KNO_3 60-40% wt) having a melting temperature of about 230°C [26] [27]. In particular, the dynamics of the thermal charging and its influence

on the thermal exchange (heat transport capacity) has been investigated. Moreover, the model has been tested in order to investigate the effect of the motion resistance parameter of the PCM during the phase change.

NOMENCLATURE

T_{sol}	[K]	solidus temperature
T_{liq}	[K]	liquidus temperature
T	[K]	temperature
H	[J/kg]	total enthalpy
h_{ref}	[J/kg]	reference enthalpy
ΔH	[J/kg]	latent heat enthalpy
c_p	[J/kgK]	specific heat at constant pressure
L	[J/kg]	latent heat of the material
A_{mush}	[kg/m^{3}s]	mushy zone constant
S	[N/m^3]	momentum source/sink term
$\vec{u}$	[m/s]	fluid velocity vector
p	[Pa]	static pressure
k	[W/mK]	thermal conductivity

Greek characters

ρ	[kg/m^3]	density of the fluid
β	[1/K]	thermal expansion coefficient
β_l	[-]	liquid fraction
M	[kg/ms]	molecular viscosity

Subscripts

ref	reference

Acronyms

TES	Thermal Energy Storage
MTES	Mobile Thermal Energy Storage
LEC	Levelized Energy Cost
PCM	Phase Change Material

2. EXPERIMENTAL SETUP

As previously said, a simple shell-and-tube geometry has been chosen for testing [29][30] (**Figure 1 Shell and tube configuration of the PCM heat storage: (a) complete system; (b) single module considered for simulations [33]**Figure 1). Thanks to the periodicity of the array of tubes in the tank, it's possible to reduce the analysis to a single module composed by an inner steel tube, in which the heat transfer fluid (HTF) flows, surrounded by a cylindrical tank filled by PCM. The module is arranged vertically, in order to trig convective flows in the liquid phase of the PCM due to buoyancy effects [31] [32]. The geometry of the experimental set-up is given in Table 1.

Table 1 - Geometry of the "tube in tank" module considered for simulations

Description	***Units***	***Value***
inner diameter of the inner tube d_{in}	mm	14
outer diameter of the inner tube d_{out}	mm	16
outer diameter of the PCM shell, D	mm	70
Length	mm	500

The properties of the PCM under consideration have been measured in the laboratory of ENEA (Italian National Agency for New Technologies, Energy and Sustainable Economic Development). Table 2 summarizes the set of properties adopted for simulation. The

temperatures T_{sol} and T_{liq} are respectively the starting and the ending point of the melting/solidification process.

The adopted HTF is “Alusil TR 50”, a silicone thermal oil; its temperature dependent properties, are provided by the manufacturer and summarized in Table 3.

The inner tube is supposed to be made of steel with a thermal conductivity of 20 W/(mK).

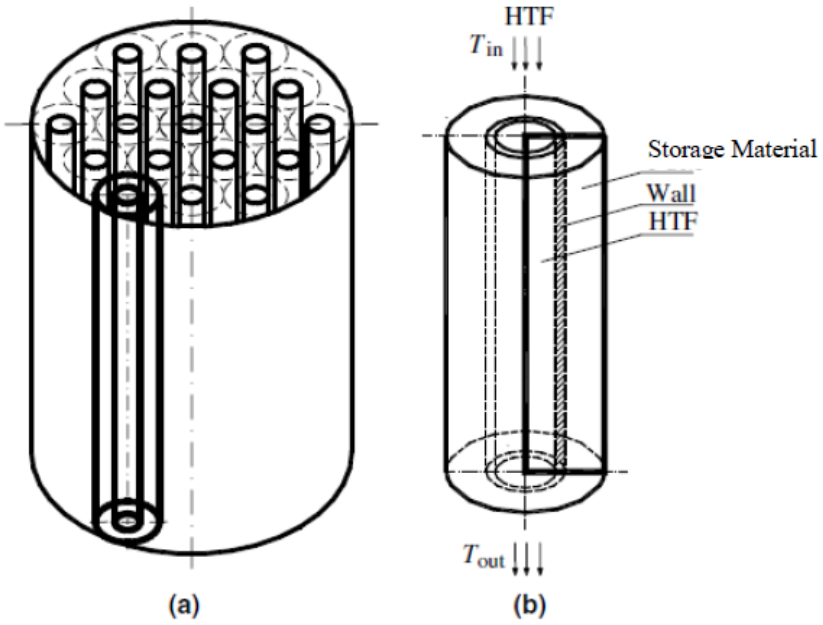

Figure 1 Shell and tube configuration of the PCM heat storage: (a) complete system; (b) single module considered for simulations [33]

Table 2 – Properties of the PCM materials where T is in °C.

Description	**Units**	**Value**
Density ($\rho_0\ computed\ at\ 150°C$)	$\mathrm{kg/m^3}$	1994.6
Thermal Expansion Coefficient	$1/\mathrm{K}$	$3.189E-4$
Thermal Conductivity	$\mathrm{W/(mK)}$	0.4886
Specific Heat solid	$\mathrm{J/(kgK)}$	1604
Specific Heat liquid	$\mathrm{J/(kgK)}$	1648
Dynamic Viscosity	$\mathrm{kg/(ms)}$	$\mu\,(T) = -4.682\ \cdot 10^{-5} \cdot T + 1.6372 \cdot 10^{-2}$
Fusion Latent Heat	$\mathrm{J/kg}$	110010
$T_{solidus}$	°C	219.88
$T_{liquidus}$	°C	244.14

.

Table 3- Properties of the HTF "Alusil TR 50" as functions of the temperature T in °C.

Description	**Units**	**Value**
Density	kg/m^3	$964.6 - 0.6458 \cdot T$
Thermal Conductivity	$W/(mK)$	$0.177 - 0.00007 \cdot T$
Specific Heat	$kJ/(kgK)$	$1.2266 + 0.0014 \cdot T$

Dynamic Viscosity	$kg/(ms)$	$17.523 \cdot T^{-1.529}$

3. GOVERNING EQUATIONS

In order to simulate the charging process of the PCM, according to the axial symmetry of the system, 2D axisymmetric CFD simulations have been carried out solving the Navier-Stokes equations together with a *Solidification and melting* model. A second order scheme has been used both for temporal and spatial discretization, in particular implicit scheme for time integration.

When a liquid phase exists in the PCM, in order to simulate the natural convection the so-called Boussinesq approximation has been considered. This model treats density as a constant value in the governing equations, except in one of the terms of the momentum equation, in which the density,ρ, varies with the temperature and it is computed taking into account a thermal expansion coefficient, β, from

$$\rho = \rho_0(1 - \beta \cdot \Delta T), \qquad (1)$$

where ΔT is the difference between the actual temperature and reference temperature T_0, at which the reference density, ρ_0 is measured.

The *Solidification and melting* model is based on the *enthalpy-porosity* technique, which defines the dynamics of the region of coexistence of both liquid and the solid phase, called *mushy zone*[34][35]. This zone is considered as a porous zone, in which the porosity is

represented by the value of the liquid fraction (β_l) ranging between 0 and 1. The liquid fraction can be defined as follows:

$$\beta_l = \begin{cases} 0 & if \quad T < T_{sol} \\ \dfrac{T - T_{sol}}{T_{liq} - T_{sol}} & if \quad T_{sol} < T < T_{liq} \\ 1 & if \quad T > T_{liq} \end{cases} \qquad (2)$$

Therefore, the following forcing term is introduced in the momentum equation:

$$S = \frac{(1 - \beta_l)^2}{({\beta_l}^3 + \epsilon)} A_{mush} \vec{u} \qquad (3)$$

In Eq. 3, the parameter ϵ is a numerical constant equal to 0.001 to prevent division by 0 (when the PCM is completely solid), $\vec{u}$ is the local velocity vector and A_{mush} is a constant called "mushy zone constant", which represents the motion resistance provided by the PCM during the phase change. S is a sink term, in the form of the Carman-Koseny equation [35] [36] [37], added to the Navier-Stokes equations to mimic the effect of pressure drop through a packed bed of solids . In the literature [31] A_{mush} values ranging from 10^3 to 10^{10} can be found. According to the Carman-Koseny equation, the dimension of the solid particles within the mushy region has the main influence on the A_{mush} value. The term *S* is maximum when the material is entirely solid ($\beta_l = 0$) and is zero when the material is liquid ($\beta_l = 1$). In the following simulations the adopted value of A_{mush} ranges from 10^5 to $5 \cdot 10^5$ kg/(m^{3}s), in order to investigate how this parameter influences the phenomenon.

In the energy equation enthalpy of PCM is computed as sum of sensible enthalpy, *h*, and latent heat, *ΔH*:

$$H = h_{ref} + \int_{T_{ref}}^{T} c_p dT + \Delta H \quad (4)$$

where

$$\Delta H = \beta_l L \quad (5)$$

Therefore the governing equations are reduced as follows:

- The mass conservation equation:

$$\nabla \cdot \bar{u} = 0 \quad (6)$$

- The momentum conservation equation:

$$\rho_0 \left(\frac{\partial \bar{u}}{\partial t} + \bar{u} \cdot \nabla \bar{u} \right) = -\nabla p + \rho \bar{g} + \bar{S} + \nabla \cdot \bar{\bar{\tau}} \quad (7)$$

where $\vec{\vec{\tau}}$ is the viscous stress tensor that, considering the fluid incompressible, is given by:

$$\bar{\bar{\tau}} = \mu[(\nabla \bar{u} + \nabla \bar{u}^T)] \quad (8)$$

where μ is the molecular viscosity.

- The energy conservation equation:

$$\frac{\partial(\rho_0 H)}{\partial t} + \nabla \cdot (\rho_0 H \bar{u}) = \nabla \cdot (k \nabla T) \quad (9)$$

4. VALIDATION

Preliminary, a validation study has been carried out with reference to the experimental work of Trp [33]. The experiment consists in a single thermal energy storage unit with an HTF pipe surrounded by a cylindrical container filled with PCM. The HTF is water and the PCM is technical grade paraffin. According to the experimental findings of Trp the PCM has a melting temperature range between 27.7°C and 35°C therefore in the present model a non-isothermal phase transition is considered. The flow rate of the HTF is 0.017 kg/s at a temperature of 45°C. The PCM has an initial temperature of 20°C and its temperature is measured during the test. Further details of the experiment are not reported here and the reader is addressed to reference paper [33]. The simulation has been carried out supposing the problem to be two-dimensional and axisymmetric. The outer walls of the tank have been supposed adiabatic. The domain has been discretized using a multi-block structured grid with orthogonal quadrilateral cells. Two grids have been considered in order to verify the solution grid independence. The grid has 3999 cells in the axial direction and, in the radial direction: about 96 cells in the PCM zone, 46 cells in the HTF zone and 8 cells in the solid steel zone. The whole grid consists of 599850 cells. In Figure 2 the comparison of the measured temperature in location 5 of the Trp experiment and numerical model with the present results are reported. The present model has a good agreement with the experimental data. Indeed the non-isothermal melting process affects the temperature increasing between the solidus and the liquidus temperature producing a changing in the slope of the curve. Moreover the convective motion of the melted phase decrease the sudden increase of temperature of the pure conductive model used by Trp. The results confirm the reliability of the numerical

approach here adopted highlighting the importance of the convective motion in reproducing the physical behavior of the melting phase.

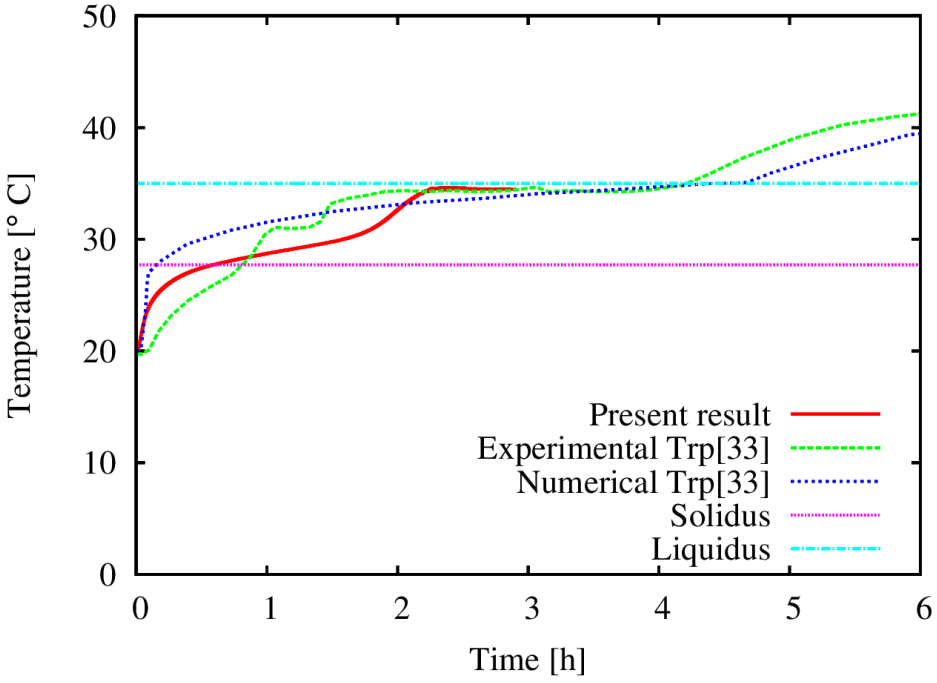

Figure 2. Comparison of the temperature recorded in x = 0.35 m, r = 0.0265 m between the present results and the results of Trp [33]

5. MESH AND OF BOUNDARY CONDITIONS

The domain has been discretized using a multi-block structured grid with orthogonal quadrilateral cells. Two grids have been considered in order to verify the solution grid independence. The coarse grid has about 2000 cells in the axial direction and, in the radial direction: about 50 cells in the PCM zone, 27 cells in the HTF zone and 4 cells in the solid steel zone. The whole grid counts about 119000 cells. In the fine grid, in the axial direction 6598 equally spaced cells have been considered and the cells have uniform axial size. Instead

in the radial direction the following cell distribution has been considered: 58 cells in the PCM region, 57 cells in the HTF region and 20 cells in the solid steel zone. The whole grid counts 681911 cells. The fine grid is shown in Figure 3.

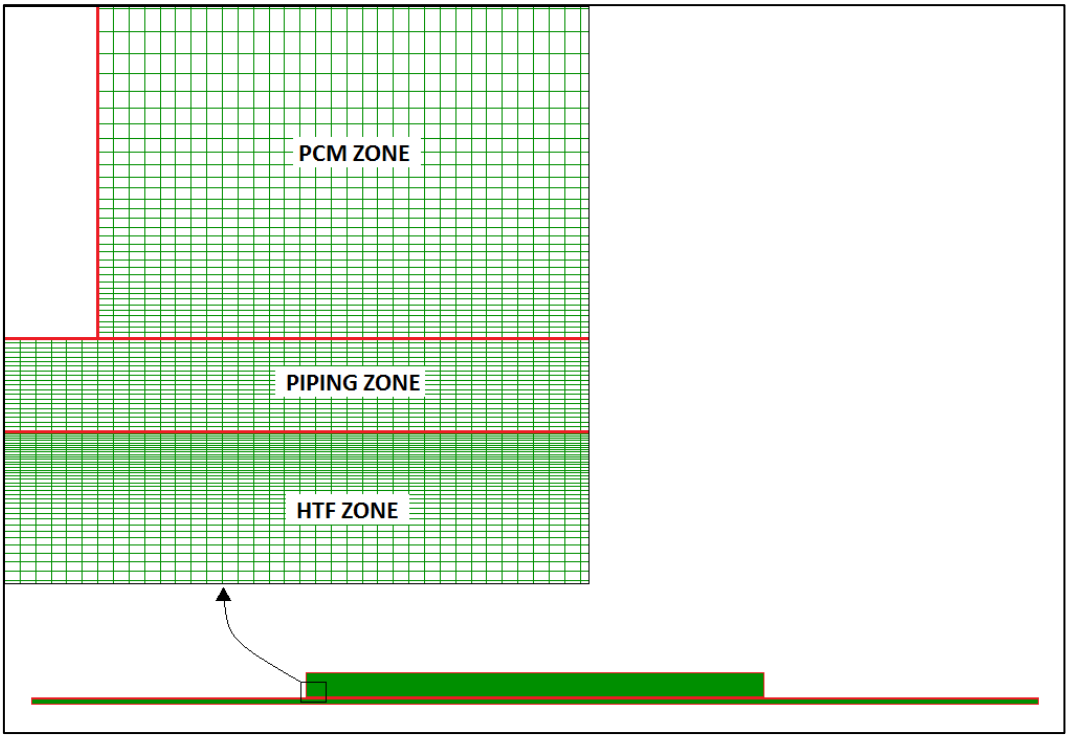

Figure 3 – Discretization of the computational domain with a zoom on the inlet of the thermal storage

The boundary conditions are as follows (see Figure 4):

- mass flow inlet at the top section of the inner tube, which imposes the HTF mass flow rate and temperature;
- outflow for the bottom section of the inner tube, this condition assumes that flow is fully-developed (the flow velocity and temperature profiles are auto similar in the flow direction;

- axis, for the centerline of the axisymmetric geometry;
- adiabatic walls for the remaining external surfaces of the tube and of the PCM;
- wall, with the thermal option Coupled, for the interface between HTF and PCM regions.

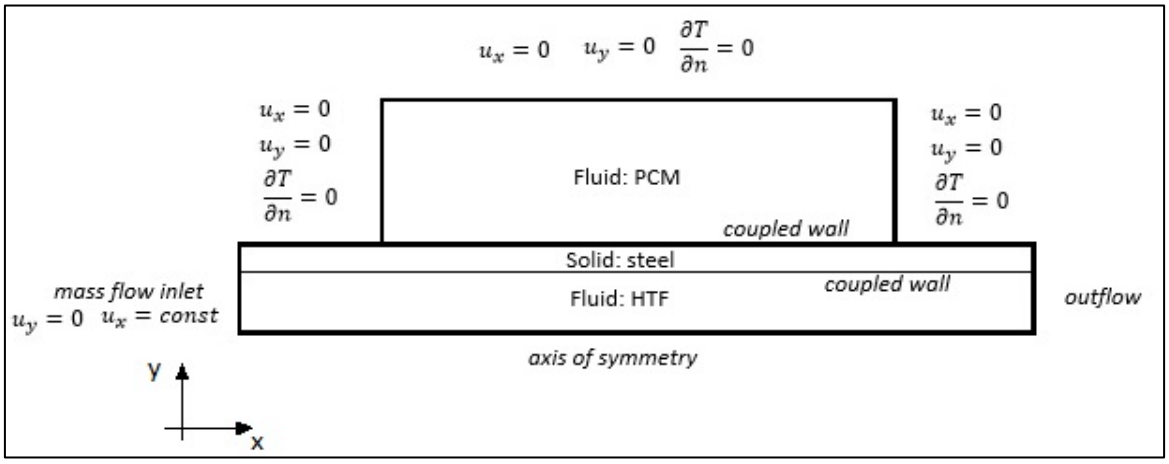

Figure 4 Schematic of the computational domain with details of the boundary conditions imposed

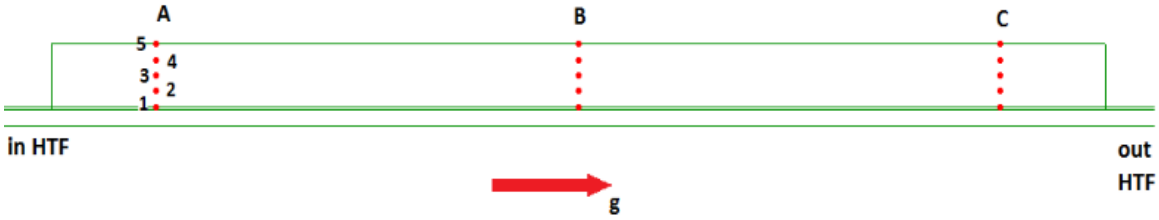

Figure 5 – Map of the probe position into the PCM

6. INITIAL AND OPERATING CONDITIONS

At the HTF mass flow inlet several user defined functions (UDF) were written in order to reproduce the features of the heater-pump group used by ENEA. During the simulation the temperature varies according to the following steps:

- Linearly increasing from 150 °C to 250 °C during the first 30 minutes.
- Kept constant at 250°C for the rest of the simulation.

The oil mass flow rate is just a function of its temperature, since the pump operates according to a constant power condition (actually the mass flow rate depends on the HTF viscosity, which is a function of its temperature). The relation between the temperature (in Kelvin) and the mass flow rate was found to be

$$\dot{m} = -10^{-6} \cdot T^2 + 1.5 \cdot 10^{-3} \cdot T - 0.358 \quad [kg/s]$$

The oil inlet is set in the upper part of the HTF tube, reproducing a vertical PCM module, which is charged from the top.

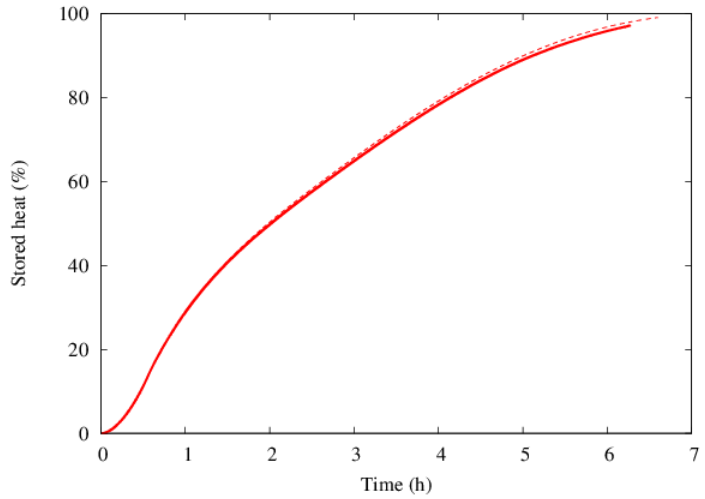

Figure 6 – Time series of the stored heat percentage. Fine grid (continuous line), coarse grid (dotted line)

During the simulation, the temperature and the liquid fraction were monitored in 15 points over the entire PCM domain. Every point is identified by a letter (index of the axial coordinate) and a number (index of the radial coordinate). A map of the probe positions is reported in Figure 5.

In Figure 6 the stored heat percentage with respect to the theoretical storable heat in the whole device is reported for two simulations with the finest and the coarsest grid. No evidences of remarkable differences is shown. Moreover in Figure 7 the temperature distribution on the PCM-HTF interface at 1h, 3h and 6h for the two different grids have been compared. The temperature distributions show no appreciable differences especially in the first phases of the melting process. There are just small differences in temperature distribution near the bottom plate for $t=6h$ (Figure 7.c) where the temperature gradients are higher. The grid independence

analysis confirms that the coarsest grid is enough reliable to solve numerically the governing equations.

7. RESULTS

The melting process has been simulated until the PCM is completely liquefied. The physical time needed for the charging process was about 6.5 hours. Globally the system have stored about 1 MJ of thermal energy.

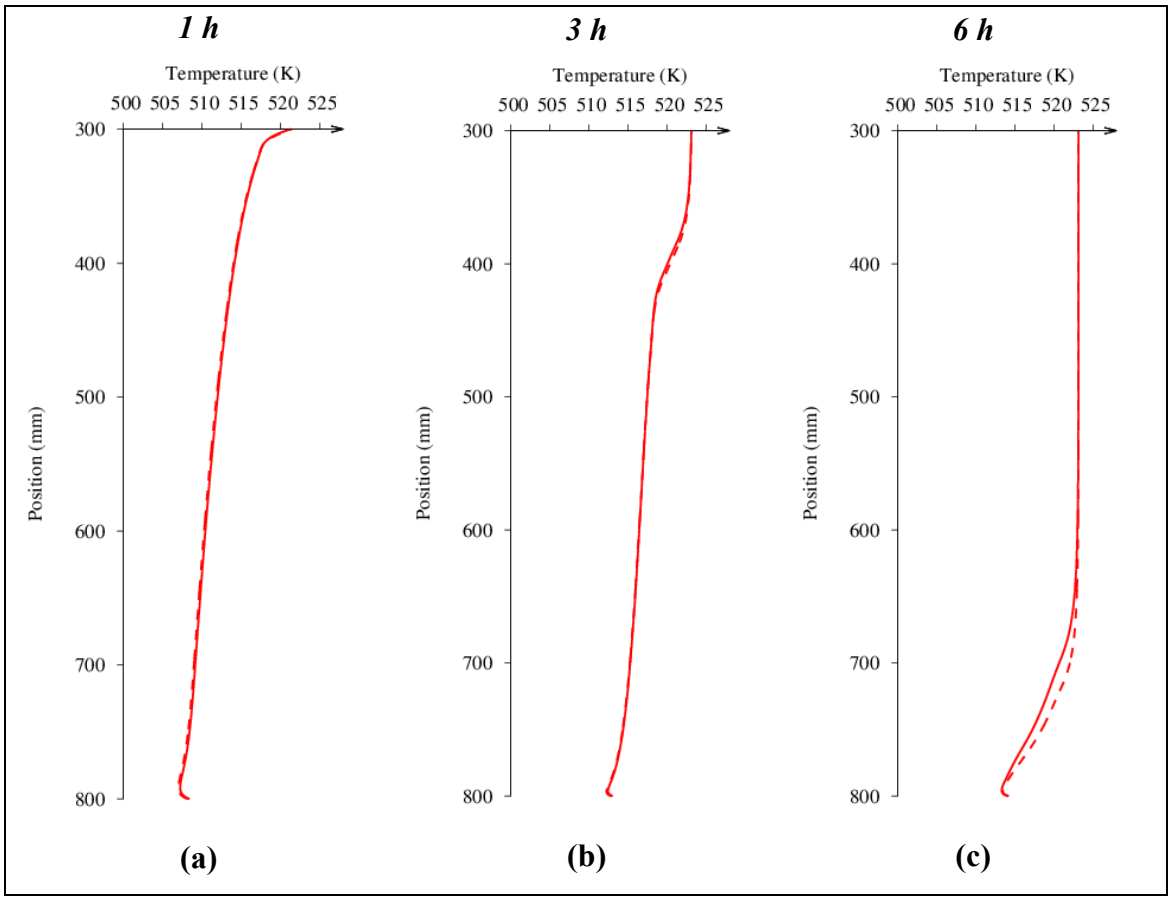

Figure 7 - Temperature distribution on the PCM-HTF interface at different instants: *t=1h* (a), *t=3h* (b), *t=6h* (c). Fine grid (continuous line), coarse grid (dotted line)

The contours of static temperature (Figure 8) and the melting front (

Figure 9) inside the PCM during the process have been monitored. Different stages of the melting process can be identified:

- initially ($t<1.h$), heat is transferred by conduction in the solid phase: the contours of static temperature are parallel to the duct wall and heat flows in radial direction according to the temperature gradients.
- In the second stage ($1.0\ h < t < 2.0h$, approximately), PCM begins to liquefy and natural convection is triggered in liquid phase. This leads to enhance the melting process in the top part as shown by the temperature profile. Heat is convectively brought upwards, as clearly shown by the picture of the liquid fraction at time of 1 hour from the start of charging. It is worth noting that convective flow is allowed in the very thin liquid layer in proximity of the wall due to the extremely low viscosity (around 0.005kg/(ms)) that characterizes the solar salts in liquid phase.
- In the third stage ($2h<t<4h$) an inclined melting front moves downwards in the upper part of the storage where PCM is completely liquid. This is due to the enhanced heat transfer due to convection. In this stage, in the lower part of the storage, the melting front moves extremely slowly in radial direction.
- In the fourth stage ($t>4h$), the melting front (perpendicular to the axis of the HTF duct) moves rapidly downwards, until the PCM is completely melted.

This behavior is similar to process described by Pal and Joshi in [38]. The analysis of time history of static temperature recorded in the monitoring points confirms such a behavior (Figure 10). It appears that temperature in all monitored points, is characterized firstly by a rapid increase due to the heat transmitted mainly by conduction in the solid phase. Then,

when the temperature limit of the solidus is reached, the rate of increase of the temperature is slowed down, due to the latent heat absorbed by the local melting process. The temperature, in this phase appears about constant, until the monitored point is reached by the melting front when the temperature rises suddenly due to convective heat exchange.

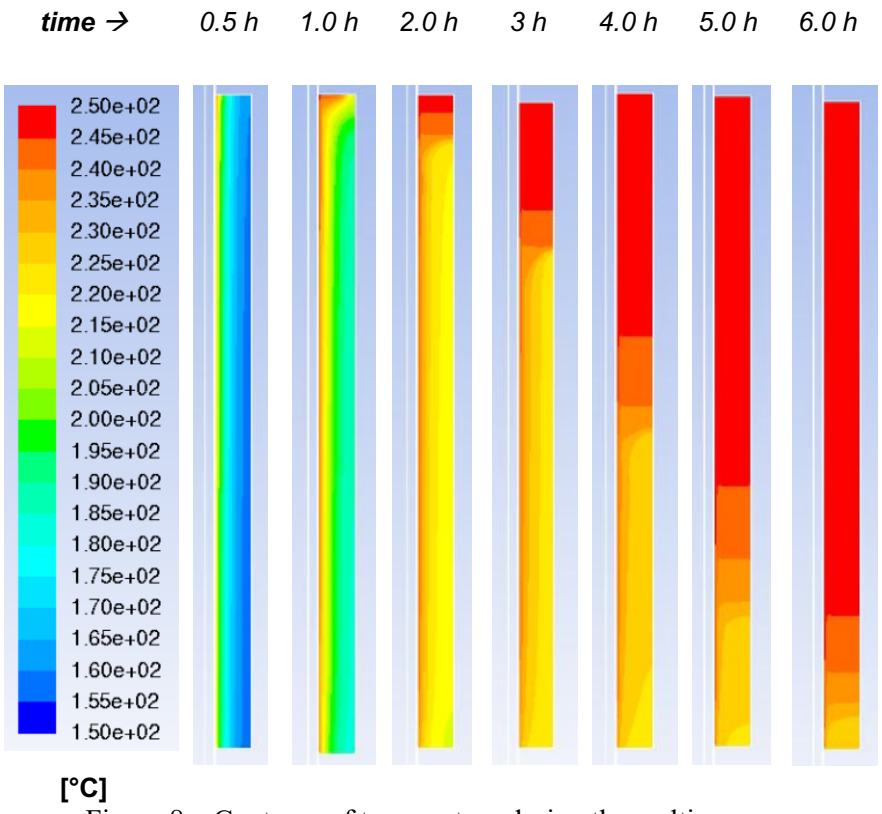

Figure 8 – Contours of temperature during the melting process

This behavior is clearly displayed in Figure 11, where the time series of temperature and liquid fraction are plotted, for one of the monitored points. The comparison of the temperature time histories at different axial locations, shows that, in the initial phase of

heating (conductive phase) the temperature rising rate depends mainly on the radial position, while the duration of the melting process is affected by the axial position since it ends when the position is reached by the melting front.

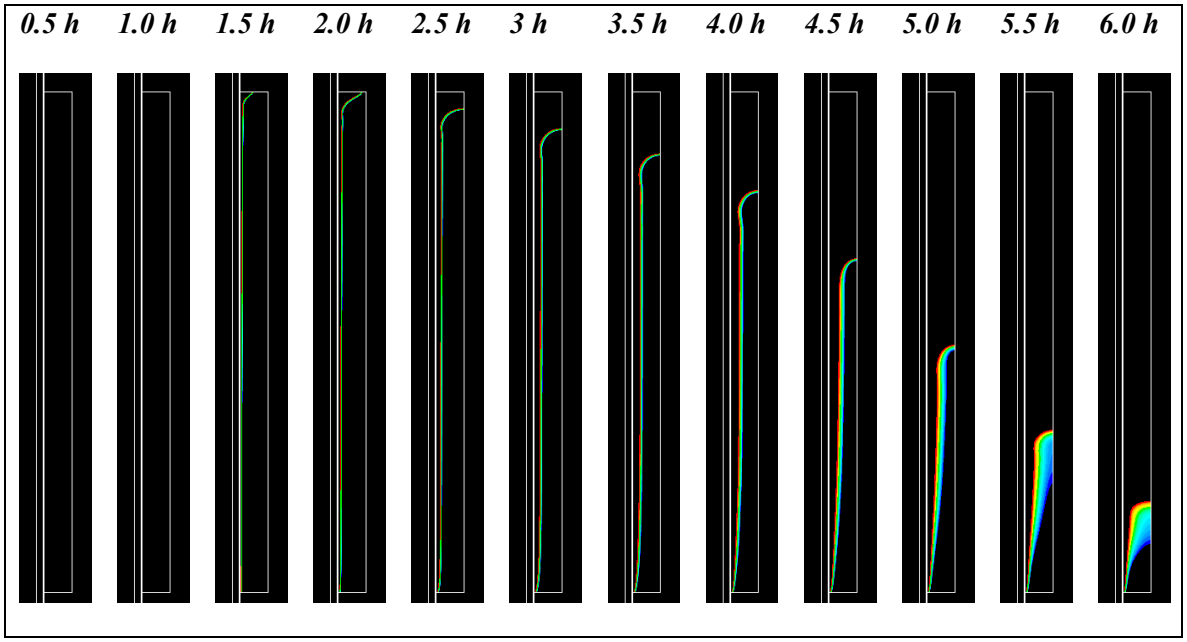

Figure 9 – Position of the melting front every 30 min

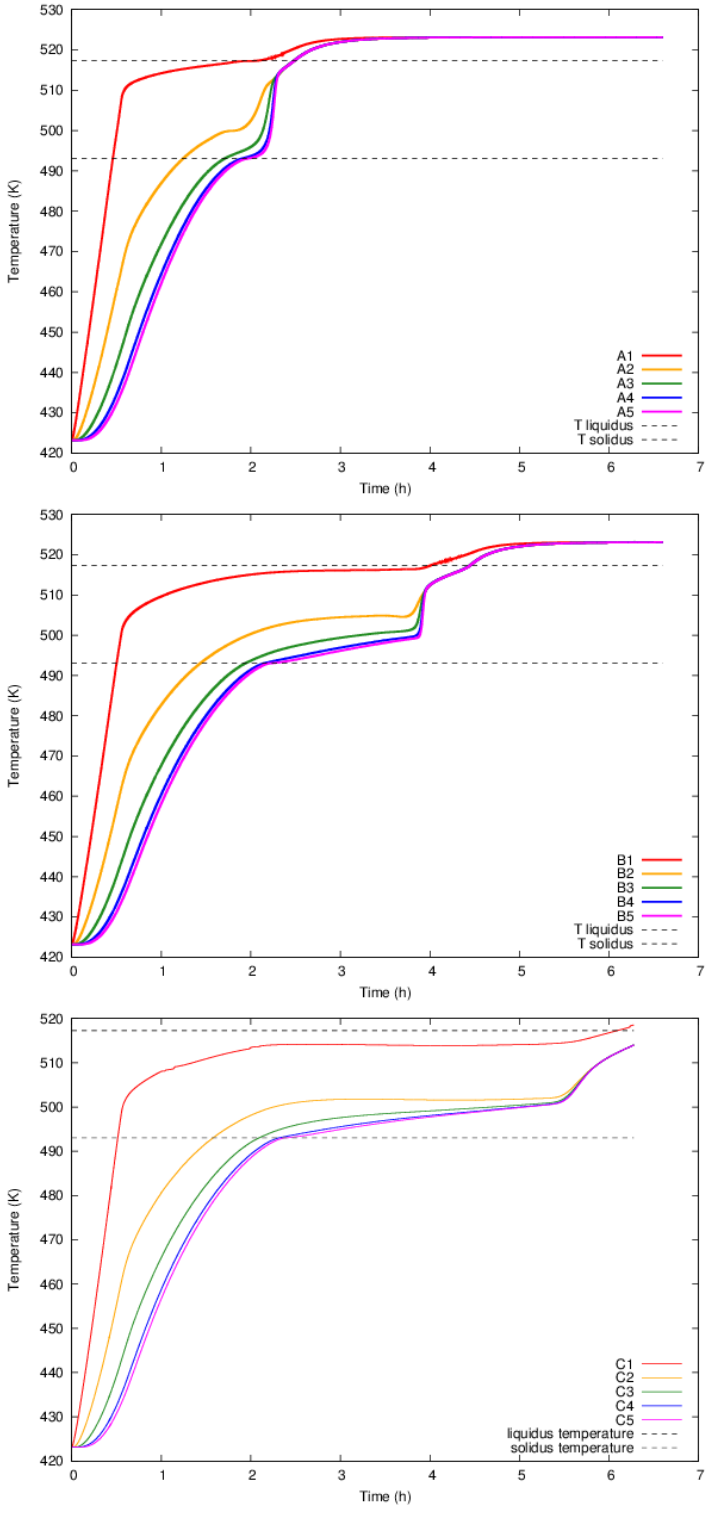

a

Figure 10 - Time series of temperature in the monitored points

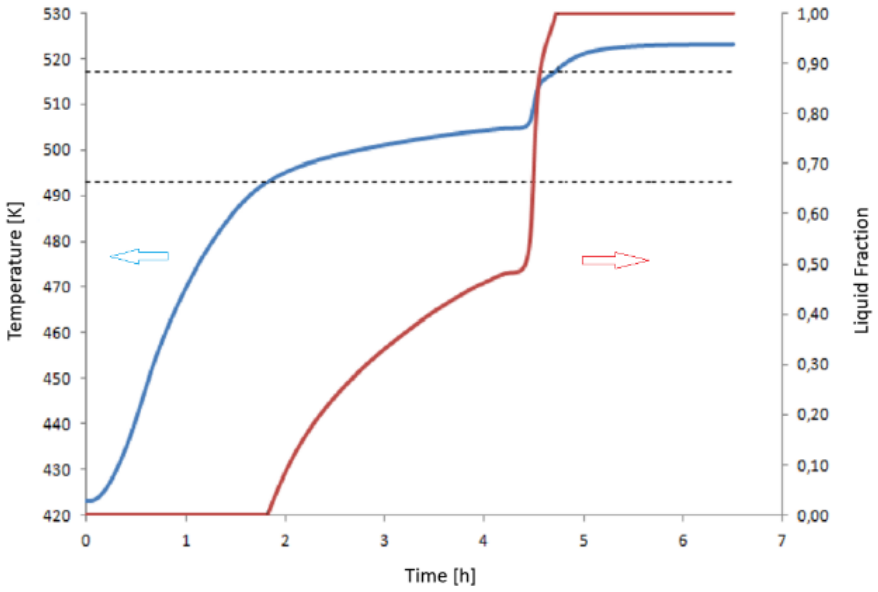

Figure 11 – Time series of temperature (blue) and liquid fraction (red)

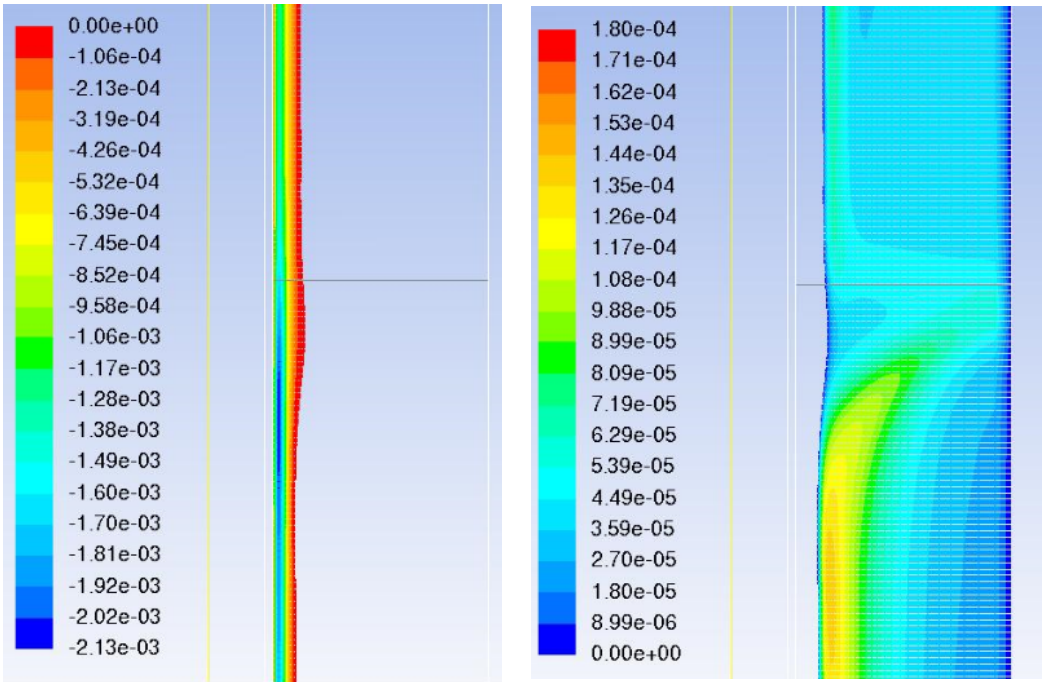

Figure 12 – Contours of axial velocity (m/s) in the middle section of the PCM . *t=4h*

The buoyancy driven flows in the liquid part of the PCM is reported in Figure 12. Distribution of axial velocity in the PCM closer to the oil tube goes up (it's hotter), while the PCM further from it goes down (because it's colder).

In order to make clear the effect of convective flows on the PCM charging process a pure conductive simulation of the heat exchange in the heat storage device has been investigated. To this purpose, the buoyancy term in the momentum equation has been set equal to zero. In this way, being the buoyancy the only forcing term in the momentum equation, the fluid motion in the PCM has been inhibited. In Figure 13 the heat flux across the vertical wall at three time instants has been reported, comparing convective and conductive cases. In the first stage (Figure 13.a), in case of convection, at $t=1h$, two peaks of the heat flux appear near the upper and lower end plates. These peaks confirms the presence of PCM motion highlighting how the PCM motion increases the heat transfer respect to the pure conductive case. In the middle phase (Figure 13.b), $t=3h$, the thicker melted zone in the PCM increases the convective heat transfer respect to the conductive case for vertical position between 400mm and 800mm. In the upper part of the PCM, between a vertical position of 300mm and 400mm, the heat transfer is reduced respect to the conductive case according to the stratification of the completely melted PCM. In Figure 13.c the most part of the PCM is liquid, therefore the upper part of the tank (between 300mm and 700mm) is stratified and stable. In case of convection, near the bottom plate the presence of melting PCM increases the temperature gradient enhancing the heat transfer respect to the case of pure conductive heat transfer.

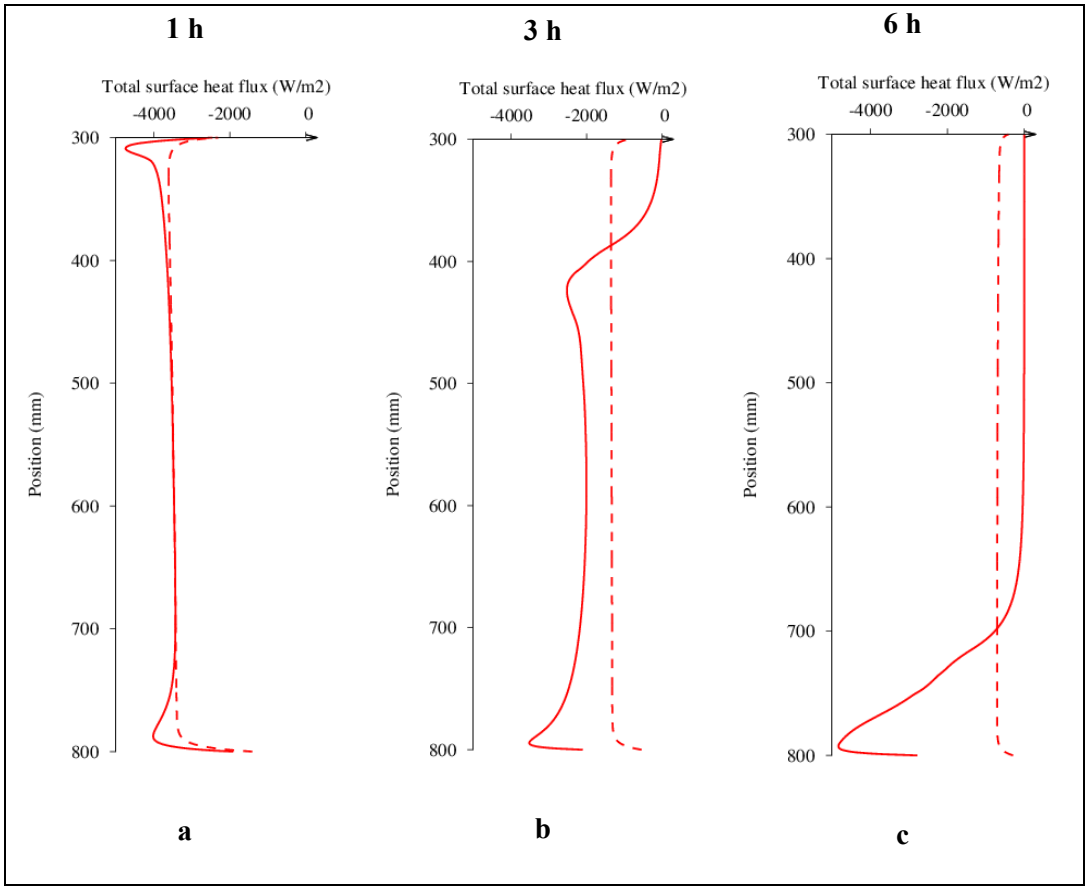

Figure 13 - Heat flux along the height of the solid duct at different instants: *t=1h* (a), *t=3h* (b), *t=6h* (c). Convective case (continuous line) and conductive case (dotted line).

In Figure 14 the time series of the stored heat, normalized with respect to the theoretical storable value, in convective and conductive cases, have been reported. In the first phase (*t<2h*) the most part of the PCM is solid, therefore there is about no difference between the two cases. Afterwards (*t>2h*), the melting of the PCM induces convective motion increasing the heat storage velocity respect to the conductive case. It is worth noting that in case of convective heat transfer, the stored heat reaches the 90% of the maximum storable heat about three hour before compared to the conductive case.

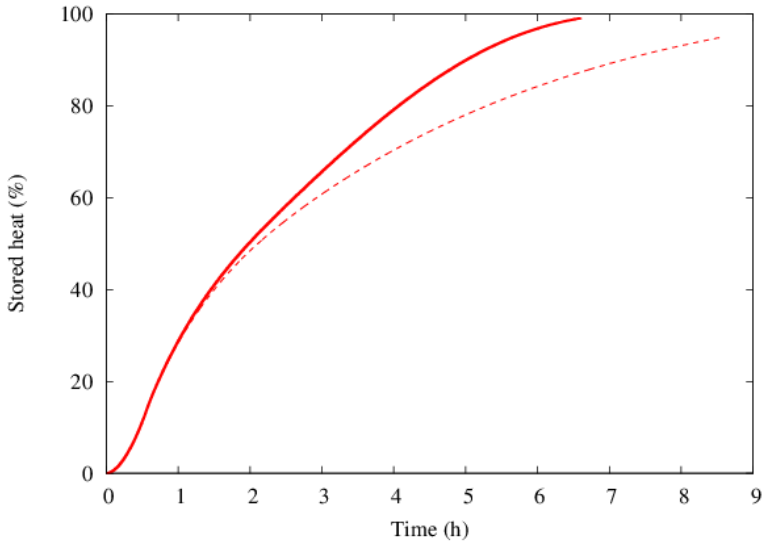

Figure 14 – Time series of the stored heat percentage. Convective case (continuous line) and conductive case (dotted line)

The influence of the constant A_{musH} is then examined. It introduces the motion resistance provided by the PCM during the phase change. In literature the mushy zone coefficient is often fixed at an higher value, about 10^5 kg/(m^{3}s) [37]. In order to evaluate its influence on the results of the charging process, numerical simulations with two values of mushy zone parameter (A_{musH}=1.0·10^5 and A_{musH}=5.0·10^5) are carried out.

Figure 15 shows that the constant A_{musH} has a little influence in the initial phases of the charging process, but influences the movement of the melting front, showing that with the highest value of the constant A_{musH}, the convective flow is slowed down. This is an important finding since, generally, in the literature it is suggested that this parameter has a little influence on the melting process. Probably, in the present work, the influence of A_{musH} is due to the low viscosity of the molten salt when they are completely melted.

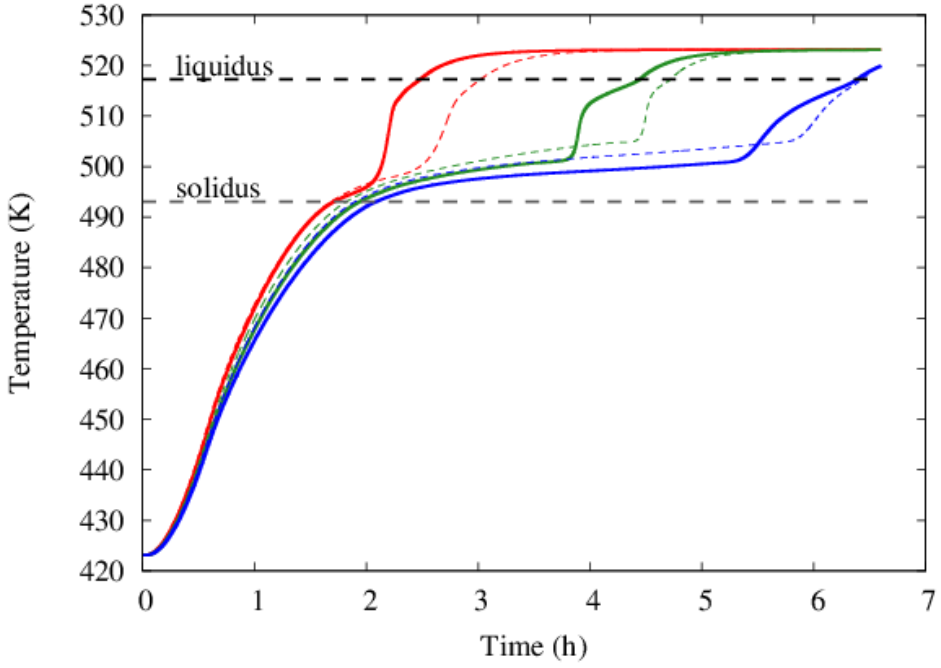

Figure 15 – Time series of static temperature at different axial positions and identical radial position (3). $\boldsymbol{A_{mush}}$=1.0·10^5 kg/(m^{3}s) (continuous line), $\boldsymbol{A_{mush}}$=5.0·10^5 kg/(m^{3}s) (dotted line)

The effects of the A_{mush} parameter is clearly reported in Figure 16 and Figure 17. Even if the total heat stored reaches the 90% at the same time (Figure 17), the dynamic of the intermediate phases is slightly different. In Figure 16 the total heat surface flux at the interface PCM-HTF highlights the influence of the mushy zone coefficient on the PCM performance. The differences are located where the melting material exist, therefor at *t=3h* the proximity of the melting interface to the PCM-HTF interface strongly influence the surface heat flux. Indeed at *t=6h* the most part of the PCM is melted, in the upper part, and it stratifies becoming stable. Further investigation on this parameter are needed in order to relate its value to a physical measured property of the PCM material.

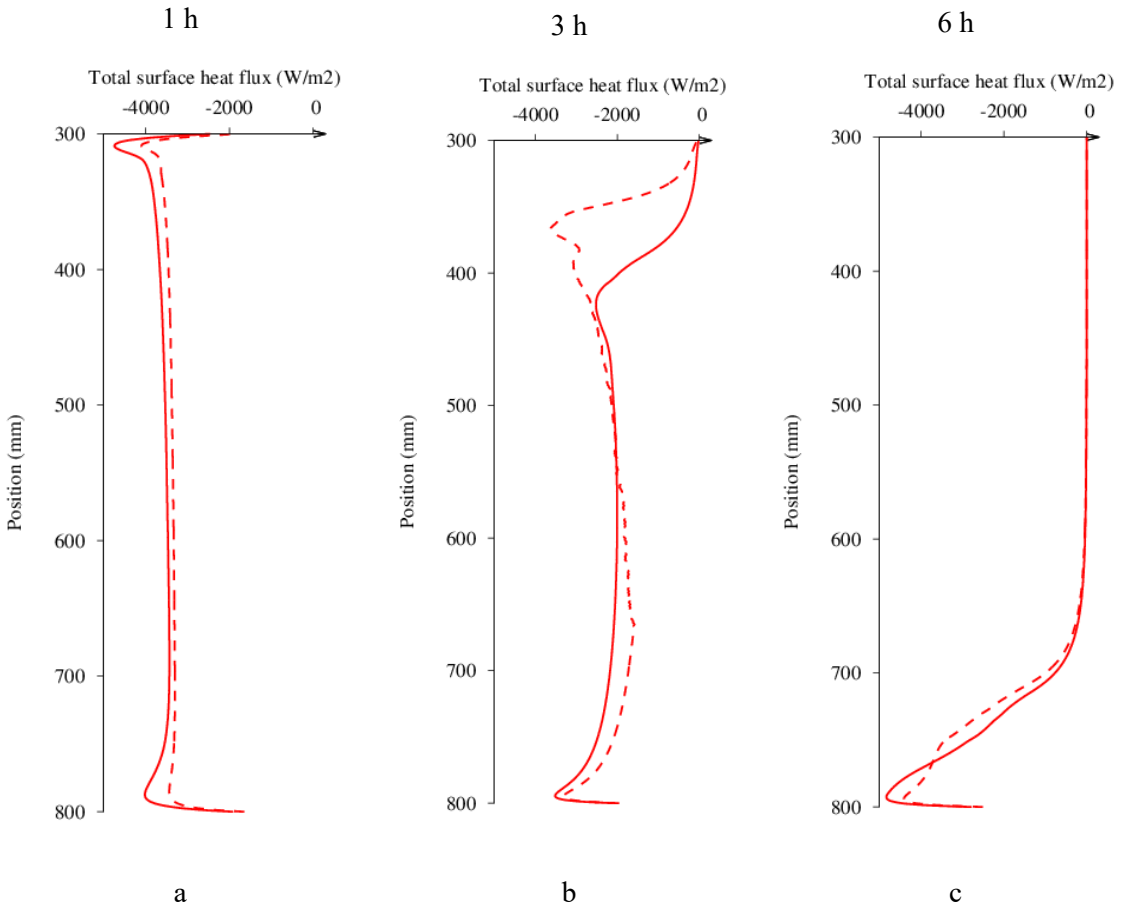

Figure 16 - Total surface heat flux along the height of the solid duct at different instants: *t=1h* (a), *t=3h* (b), *t=6h* (c). $\boldsymbol{A_{musk}}$=1.0·10^5 kg/(m^{3}s) (continuous line), $\boldsymbol{A_{musk}}$=5.0·10^5 kg/(m^{3}s) (dotted line)

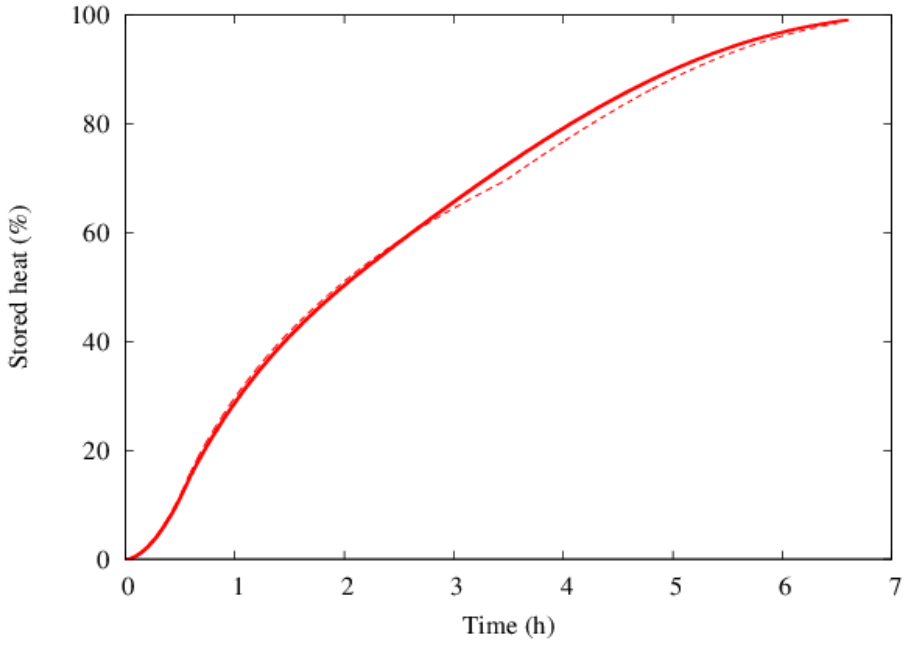

Figure 17 - Stored heat percentage. $\boldsymbol{A_{mush}}$=1.0·10^5 kg/(m^{3}s) (continuous line), $\boldsymbol{A_{mush}}$=5.0·10^5 kg/(m^{3}s) (dotted line)

5 CONCLUSIONS

Numerical simulations of the melting process in a shell and tube latent heat storage has been investigated. The simulation set up is based on experimental devices developed by ENEA for applications to high temperature concentrated solar power plants. An analysis on the convection effect on the heat transfer respect to a pure conductive model, in which the buoyancy has been trigged off, has been reported. The study confirms that the convective motion increases the heat flux to the PCM reducing the heat storage time. Details on the buoyancy driven flows within the PCM is reported highlighting how the fluid motion increases the temperature gradient at the PCM-HTF interface respect to the conductive case.

The results show that the heat storage phase is completed three hours earlier respect the pure conductive simulation.

Moreover the effect of the motion resistance parameter of the PCM during the phase change has been investigated. Even though, in the explored range, the total storage time is not affected by the parameter change, a delay in the triggering of the convective flows has been found. Indeed this preliminary study remarks that the influence of the motion resistance parameter (A_{mush}) is not negligible in this case, despite usually in the literature it is suggested that this parameter should have a little influence on the melting process.

ACKNOWLEDGEMENTS

This work was supported by the 2013 Annual Research Plan (PAR2013) of the Electric System Research Program (RSE) of the Italian Minister of the Economic Development. The financial support of the PON02_00323_3588749 "SMART ENERGY BOXES (SEB)" is also gratefully acknowledged.

REFERENCES

[1] IEA International Energy Agency: World Energy Outlook 2011. Paris; 2011.

[2] IEA International Energy Agency: Technology Roadmap. Solar Heating and Cooling. Paris; 2012.

[3] Hasnain SM: Review on sustainable thermal energy storage technologies. Part I: Heat Storage Materials and techniques. Energ Convers Manage 1998, 39(11):1127-1138.

[4] Herrmann U, Kearney DW: Survey of thermal energy storage for parabolic trough power plants. J Sol Energy Eng 2002, 124(2):145-152.

[5] Laing D: Solar thermal energy storage technologies. Energy Forum 10000 Solar Gigawatts Hannover 2008

[6] Pizzolato A, Donato F, Verda V, Santarelli M: CFD-based reduced model for the simulation of thermocline thermal energy storage systems. Applied Thermal Engineering 2015, 76: 391–399

[7] Aydin D, Utlu Z, Kincay O (2015): Thermal performance analysis of a solar energy sourced latent heat storage. Renewable and Sustainable Energy Reviews, 50, 1213–1225.

[8] Gil A, Medrano M, Martorell I, Lazaro A, Dolado P, Zalba B, Cabeza LF: State of the art on high temperature thermal energy storage for power generation. Part 1-Concepts, materials and modellization. Renew Sust Energ Rev 2010, 14:31–55.

[9] Kuznik F, David D, Johannes K, Roux J: A review on phase change materials integrated in building walls. Renew Sust Energ Rev 2011, 15:379-391.

[10] Cabeza LF, Castell A, Barreneche C, de Gracia A, Fernández AI: Materials used as PCM in thermal energy storage in buildings: A review. Renew Sust Energ Rev 2011, 15:1675–1695.

[11] Baetens R, Jelle BP, Gustavsen A: Phase change materials for building applications: a state-of-the-art review. Energ Buildings 2010, 42:1361-1368.

[12] Roskilly AP, Taylor PC, Yan J, Energy storage systems for a low carbon future – in need of an integrated approach. Applied Energy 2015, 137:463-466.

[13] Sciacovelli A, Gagliardi F, Verda, V. Maximization of performance of a PCM latent heat storage system with innovative fins. Applied Energy 2015, 137, 707–715.

[14] Li H, Wang W, Yan J, Dahlquist E, Economic assessment of the mobilized thermal energy storage (M-TES) system for distributed heat supply, Applied Energy 2013, 104: 178-186.

[15] Wang W, Li H, Guo S, He S, Ding J, Yan J, Yang J, Numerical simulation study on discharging process of the direct-contact phase change energy storage system. Applied Energy 2015, 150: 61-68.

[16] Guo S, Li H, Zhao J, Li X, Yan J, Numerical simulation study on optimizing charging process of the direct contact mobilized thermal energy storage. Applied Energy 2013, 112: 1416-1423.

[17] Nuytten T, Classens B, Paredis K, Bael JV, Six D: Flexibility of a combined heat and power system with thermal energy storage for district heating. Applied Energy 2013, 104: 583-591

[18] Wang WL, He SQ, Guo SP, Yan J, Ding J A combined experimental and simulation study on charging process of erythritol-HTO blending based energy storage system. Energy Convers Manage 2014, 83:306-313

[19] Sharma A, Tyagi VV, Chen CR, Buddhi D: Review on thermal energy storage with phase change materials and applications. Renew Sust Energ Rev 2009, 13:318–345.

[20] Sharma SD, Sagara K: Latent heat storage materials and systems: a review. Int J Green Energy 2005, 21–56.

[21] Fan LW, Khodadadi JM, Thermal conductivity enhancement of phase change materials for thermal energy storage: a review, Renew. Sust. Energy Rev. 15 (2011) 2446.

[22] Zhao CY, Wu ZG, Heat transfer enhancement of high temperature thermal energy storage using metal foams and expanded graphite, Sol. Energy Mater. Sol. C 95 (2011) 636-643

[23] Seddegh S, Wang X, Henderson AD: Numerical investigation of heat transfer mechanism in a vertical shell and tube latent heat energy storage, Applied Thermal Engineering, vol. 87 (2015) 698-706

[24] Tamme R, Bauer T, Buschle J, Laing D, Muller-Steinhagen H, Steinmann WD: Latent heat storage above 120°C for applications in the industrial process heat sector and solar power generation. Int J Energ Res 2008, 32:264–271.

[25] Sarı A, Karaipekli A: Preparation, thermal properties and thermal reliability of palmitic acid/expanded graphite composite as form-stable PCM for thermal energy storage. Sol Energ Mat Sol C 2009, 93:571–576.

[26] Farid MM, Khudhair AM, Razack SAK, Al-Hallaj S: A review on phase change energy storage: materials and applications. Energ Convers Manage 2004, 45:1597–1615.

[27] Sharma A, Tyagi VV, Chen CR, Buddhi D: Review on thermal energy storage with phase change materials and applications. Renew Sust Energ Rev 2009, 13:318–345.

[28] Kenisarin MK: High-temperature phase change materials for thermal energy storage. Renew Sust Energ Rev 2010, 14:955–970.

[29] Lacroix M: Numerical simulation of a shell-and-tube latent heat thermal storage unit. Solar Energy, vol. 50, N_o 4 (1993) 357-367

[30] Esam M. Alawadhi: Phase change process with free convection in a circular enclosure: numerical simulation. Computers & Fluid 33 (2004) 1335-1348

[31] Shmueli H, Ziskind G, Letan R: Melting in a vertical cylindrical tube: numerical investigation and comparison with experiments. Internation Journal of Heat and Mass Transfer 53 (2010) 4082-4091

[32] Longeon M, Soupart A, Fourmigué JF, Bruch A, Marty P: Experimental and numerical study of annular PCM storage in the presence of natural convection. Applied Energy 112 (2013) 175-184

[33] Anica Trp: An experimental and numerical investigation of heat transfer during technical grade paraffin melting and solidification in a shell-and-tube latent thermal energy storage unit. Solar Energy, 2005.

[34] Boo JH, Lee SK, Kim JK: Numerical analysis of a thermal storage system with inserted heat pipes for medium-high temperature range. International Heat Pipe Symposium, 2011.

[35] V. R. Voller and C. Prakash, A fixed grid numerical modelling methodology for convection diffusion mushy region phase-change problems, Int. J. Mass. Tranfer 30 (8), pp. 1709-1719,1987.

[36] V. R. Voller, M. Cross and N. C. Markatos, An enthalpy method for convection/diffusion phase field models of solidification, Int. J. Num. Methods. Eng. 24 (1), pp. 271-284, 1987.

[37] Brent AD, Voller VR, Reid KJ: Enthalpy-porosity technique for modeling convection-diffusion phase change: application to the melting of a pure metal, Numerical Heat Transfer 13 (1988) 297-318.

[38] Debabrata P, Yogendra KJ: Melting in a side heated tall enclosure by a uniformly dissipating heat source, International Journal of Heat and Mass Transfer 44 (2001) 375-387

[39] Fortunato B, Camporeale SM, Torresi M, Albano M: Simple mathematical model of a thermal storage with PCM, AASRI Procedia, vol.2 (2012) 241-248.